Trajectory Adaptation for an Impedance Controlled Cooperative Robot According to an Operator's Force

Yousefizadeh, Shirin; Méndez, Juan de Dios Flores; Bak, Thomas

Published in:
Automation in Construction

DOI (link to publication from Publisher):
10.1016/j.autcon.2019.01.006

Publication date:
2019

Document Version
Accepted author manuscript, peer reviewed version

Citation for published version (APA):
Yousefizadeh, S., Méndez, J. D. D. F., & Bak, T. (2019). Trajectory Adaptation for an Impedance Controlled Cooperative Robot According to an Operator's Force. *Automation in Construction*, *103*, 213-220. https://doi.org/10.1016/j.autcon.2019.01.006

Trajectory Adaptation for an Impedance Controlled Cooperative Robot According to an Operator's Force

Shirin Yousefizadeh[1,*]

Department of Electronic Systems, Aalborg University, Aalborg, Denmark

Juan de Dios Flores Mendez[2]

Department of Electronic Systems, Aalborg University, Aalborg, Denmark

Thomas Bak[3]

Department of Electronic Systems, Aalborg University, Aalborg, Denmark

Abstract

The goal of this paper is to design a controller for a cooperative robot based on a human's force that makes the robot's end-effector follow predefined motion primitives. To this aim, based on a 3D model of the robot, the kinematics and dynamics are analyzed at first. Then, an automatic online trajectory generator is designed based on the pre-defined motion primitives and the human operator intention detection. The generated trajectory serves as an input to an impedance controller. The designed impedance controller makes the robot achieve an active compliance for a safe cooperation with the human operator. The proposed controller is implemented on a robot, namely WallMoBot, which is a cooperative robot for heavy glass panels installation. Simulations of the proposed method are presented, and the results show that the method is well suited for the WallMoBot.

Keywords: Cooperative robots, Impedance control, Online trajectory generation, Safe physical human-robot interaction (pHRI), Motion primitives, Construction robots.

1. Introduction

Traditional industrial robots are used in known environments or have cages around them to prevent damage to humans and the workspace. Safety

requirements for industrial robot applications are developed by the International Organization for Standardization (ISO) and specified in ISO 10218-1 and ISO 10218-2. Conventional industrial applications are limited to motion-control tasks. Nonetheless, close cooperation between humans and robots is a necessity for many new robotic applications such as assistive robots for elderly people [1], for surgery [2, 3], or for construction [4]. Cooperation between humans and robots may entail benefits for the operator's health [5]. Also, human-robot cooperation enables combining human dexterity and robot strength, which might improve work efficiency [6]. In physical human-robot interaction, ensuring the safe operation of the robot manipulator is of great importance. Safety standards for collaborative operations are provided in the technical specification ISO/TS 15066. Also, physical human-robot cooperation tasks involve interaction forces between the robot and the human operator and/or the environment. Compliant motion is the ability of a robot to follow a trajectory in a manipulation task that involves these interaction forces. This compliant behaviour can be attained in either a passive mode or an active mode. While passive interaction control is related to the inherent structural compliance of the robot, active interaction control relies on a designed control system to attain compliance [4]. Force control can be achieved via admittance or impedance control. These methods have complementary characteristics [7]. However, admittance control might exhibit stability issues [8]. The so called impedance control is an indirect force control strategy because it does not require contact force measurements [9]. Mechanical impedance is defined as the ratio of the generalized force to the generalized velocity [10], and it can be described by an equivalent mass-spring-damper system with adjustable parameters [4]. Impedance control aims to impose a desired mechanical impedance on the robot at the contact point of the robot with the human operator [11] according to the applied force from the human operator. Then, the robot can move based on the imposed mechanical impedance. This movement can be done based on predefined motion primitives.

Motion primitives are basic motion elements whose complex movements can be generated by their combination [12]. Motion primitives can provide a simple and intuitive user interface. They benefit the performance of repetitive movements such as handwriting [13], choreographed quadrocopter flight [14] or automating repetitive surgical subtasks [15]. In [16], some motion primitives are defined for installation of glass panels.

The installation of the glass panels has been usually done by two or more

workers by manually lifting the glass panels. Another installation method employs a joystick to control a robot end-effector to move it in operational space to the position of installation [16]. The manual installation of the glass panels induces a large load to the joints and the back of the workers that can cause a serious injury. On the other hand, the joystick controlled robot has several drawbacks such as non-intuitive control and large installation time for accurate positioning. The WallMoBot is a construction robot designed to cooperate with the human operator to lift, transport and install glass panels of up to 150 kg with an accuracy of 1.5 mm safely and effectively. The Requirements for construction robots are to be able to handle relative heavy loads, also to move and adjust motions in a dynamic environment [17].

Our proposal is to control the large movements of the glass panel with a joystick and to control the fine movements manually, i.e., the operator will grab the glass panel and move it to the desired position. In this way, the WallMoBot combines the abilities of joystick controllers with the dexterity of the human operator. We believe that this method will decrease the installation time while increasing the precision. The WallMoBot must also be able to track the motion of the glass panel according to the exerted external forces to its end-effector, when the human opertor interacts with the glass panel. Therefore, the tracked trajectory must be adjusted online based on the human operator intention [18]. In addition, the tracked trajectory is aimed to replace the defined motion primitives for WallMoBot, i.e. *move*, *slide*, *lift* in [16].

In this paper, we focus on the second stage of glass installation, with fine movements. The aim is to develop a control strategy for the WallMoBot to handle large glass panels. An impedance controller is developed in order to achieve the physical human robot interaction with the desired mechanical impedance. The main contribution of this paper, which has not been addressed before, is that the designed impedance controller is interconnected with an online trajectory generator that substitute the previously defined motion primitives, i.e. *move*, *slide*, *lift*. The trajectory generator adjusts and generates a trajectory in real-time, according to the force originated from the human robot interaction. The trajectory generation algorithm complies with safety requirements.

The outline of this paper is as follows. Section II presents the modelling of the WallMoBot. Then the proposed impedance controller for force control in WallMoBot is provided in Section III. The illustrative simulation results are described in section IV. Finally, in section VI, the conclusion and discussion

of future work are presented.

2. The Robot Model

The WallMoBot consists of a manipulator with 6 degrees of freedom (DOF) installed on a mobile platform which is shown in Fig. 1. The coordinate frames $o_i x_i y_i z_i, \forall \in \{0, ..., 6, 7, e\}$, are assigned to the robot complying with the Denavit-Hartenberg (DH) convention and they are visualized in Fig. 1. Coordinate frames 0 and e denote the base frame and the end-effector frame, respectively, and coordinate frame 3 is associated with the parallelogram link which keeps the same orientation as the base frame.

In this paper, we consider the robot is planar, i.e., the generalized coordinates q_1, q_5, q_6 are assumed to be zero and only the coordinates $q_2,\ q_3,\ q_4$, as shown in Fig. 1, are used. In other words, only three degrees of freedom of the robot are considered. The DH parameters of the WallMoBot from the Base frame to the end-effector frame are given in Table 1. In addition, the value of the DH parameters along with the other parameters required to obtain the kinematics of the robot are listed in Table 2.

Table 1: Link parameters of the WallMoBot given in the modified DH representation, where q_i are the generalized coordinates.

i	a_{i-1} [m]	d_i [m]	$\theta_i = q_i$+offset [rad]	α_{i-1} [rad]
1	0	0	$q_1 + 0$	0
2	a_1	0	$q_2 - \pi/2$	$-\pi/2$
3	a_2	0	$-q_2 + \gamma$	0
4	a_3	0	$q_3 + \pi/2 - \gamma$	0
5	a_4	0	$q_4 + \pi/2$	0
6	a_5	d_6	$q_5 + \pi/2$	$\pi/2$
7	0	0	$q_6 - \pi/2$	$-\pi/2$

Remark: In this paper, $c_i = \cos(q_i)$, $s_i = \sin(q_i)$, $s_{ij} = \sin(q_i + q_j)$, and $c_{ij} = \cos(q_i + q_j)$.

The forward kinematics of the robot is described using the following ho-

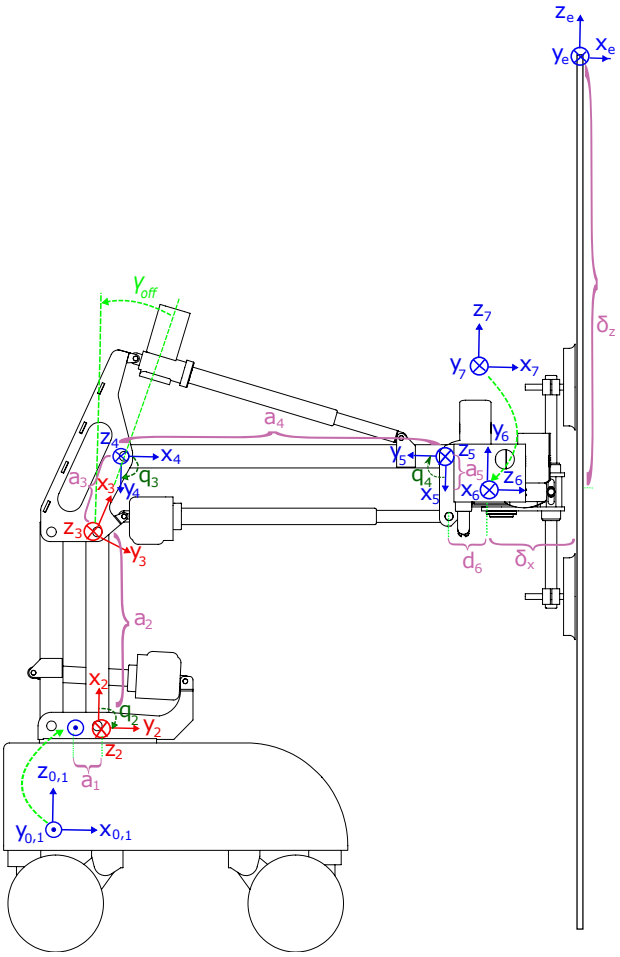

Figure 1: Illustration of the generalized coordinates of the WallMoBot. Frame 0 coincides with frame 1 when q_1 is zero.

mogeneous transformation matrix:

$$ {}^{0}_{e}T\Big|_{q_1=q_5=q_6=0} = \begin{bmatrix} c_{34} & 0 & s_{34} & \boldsymbol{x} \\ 0 & 1 & 0 & 0 \\ -s_{34} & 0 & c_{34} & z \\ 0 & 0 & 0 & 1 \end{bmatrix} \tag{1} $$

Table 2: Required parameters for obtaining the WallMOBot kinematics. * This value can be changed based on the size of the glass panel.

Symbol	Parameter	Value
a_1	Horizontal distance between frame 1 and frame 2	0.06 [m]
a_2	Length of link 2	0.5 [m]
a_3	Length of link 3	0.195 [m]
a_4	Length of link 3	0.85 [m]
a_5	Length of link 3	0.093 [m]
d_6	Length of link 3	0.109 [m]
γ_{off}	Offset angle between frame 2 and 3	0.3458 [rad]
δ_z	Height of the glass panel from the attachment point to the top	1.5* [m]
δ_x	Distance of the glass panel from the final joint of the robot	0.2025 [m]

where,

$$\begin{aligned} \boldsymbol{x} &= a_1+(d_6+\delta_x)c_{34}+(\delta_z-a_5)s_{34}+a_4c_3+a_3s_{\gamma_{off}}+a_2s_2 \\ z &= a_3c_{\gamma_{off}} - (d_6+\delta_x)s_{34} + (\delta_z-a_5)c_{34} + a_2c_2 - a_4s_3 \end{aligned} \quad (2)$$

Based on the above homogeneous transformation, the pose of the end effector x_e can be described by the following map:

$$k(q) : (q_2, q_3, q_4) \rightarrow x_e = \begin{bmatrix} \boldsymbol{x} \\ z \\ \theta \end{bmatrix} = \begin{bmatrix} a_1 + (d_6+\delta_x)c_{34} + (\delta_z - a_5)s_{34} + a_4c_3 + a_3s_{\gamma_{off}} + a_2s_2 \\ a_3c_{\gamma_{off}} - (d_6+\delta_x)s_{34} + (\delta_z-a_5)c_{34} + a_2c_2 - a_4s_3 \\ q_3 + q_4 \end{bmatrix} \quad (3)$$

The dynamic model of the robot is computed using Lagrange formulation. The Lagrange equations are expressed as

$$\frac{d}{dt}\left(\frac{\partial \mathcal{L}}{\partial \dot{q}}\right)^T - \left(\frac{\partial \mathcal{L}}{\partial q}\right)^T = \zeta \quad (4)$$

where q is a vector of generalized coordinates, ζ is a vector of generalized

torques, and L is the Lagrangian of the mechanical system defined as

$$L(q, \dot{q}) := T(q, \dot{q}) - U(q) \tag{5}$$

where $T(q, \dot{q})$ is the kinetic energy and $U(q)$ is the potential energy of the system.
Deriving the Lagrange equations, the dynamic model of the robot can be obtained as

$$B(q)\ddot{q} + C(q, \dot{q})\dot{q} + F_f(\dot{q}) + g(q) + \tau_{ext} = \tau \tag{6}$$

where $B(q)$ is the symmetric inertia matrix, $C(q, \dot{q})$ is the matrix of centrifugal, and Coriolis terms, $g(q)$ contains the gravity terms, $F_f(\dot{q})$ represents viscous and columb friction torques, and τ_{ext} is the involved interaction torque in the joint space in the cooperation task between the human operator and the robot.
Notation: For the sake of brevity, the arguments q and $\dot{q}$ are removed from $B(q)$, $C(q, \dot{q})$, $F_f(\dot{q})$, and $g(q)$.

3. Online trajectoy generator interconnected to an Impedance Controller

In the cooperative task between the human operator and the WallMoBot, as shown in Fig. 2, the human operator applies a force to the glass which is transmitted to the end-effector of the robot via the glass. Then, the robot movement caused by the human force is controlled by the impedance control. The proposed control strategy is based on identifying online minimum jerk trajectories to be tracked by the end-effector, and a computed-torque controller to track the defined trajectories with a desired impedance of the robot along these trajectories. The considered control strategy is illustrated in Fig. 3. The function of the outer loop is to transform the human force into the desired position error. To implement this control strategy, interaction force, as well as the joints positions and velocities are required.

The blocks and parameters in the Fig. 3 are explained thereafter.

3.1. Computed-Torque Control

Computed torque controller is a kind of feedback linearization of nonlinear systems technique [19]. It linearizes the nonlinear motion equations based

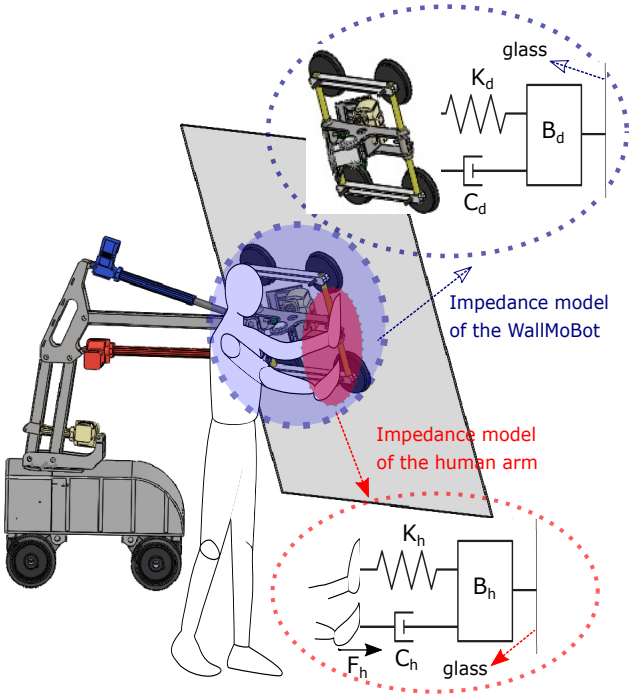

Figure 2: Human-WallMoBot cooperation.

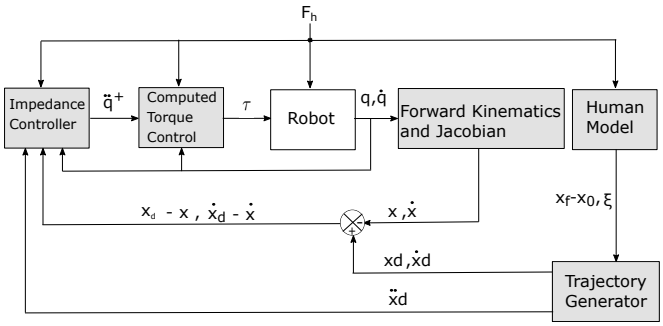

Figure 3: Impedance control block diagram.

on the the so-called *computed-torque control law* equation [20] as

$$\tau = B\ddot{q}^{+} + C\dot{q} + F_f + g \tag{7}$$

where, $\ddot{q}^{+}$ is given by the impedance controller explained below.

3.2. Impedance Controller

The first step to implement the impedance control is to determine a desired behaviour of the robot. As can be seen in (6), the dominant behavior of the robot dynamic is a second order system. Therefore, the desired impedance is usually considered as a system with order two as

$$B_d(\ddot{x} - \ddot{x_d}) + C_d(\dot{x} - \dot{x_d}) + K_d(x - x_d) = -F_h \tag{8}$$

where, $x = \begin{bmatrix} \boldsymbol{x} & z & \theta \end{bmatrix}^T$, F_h is the human force/torque applied to the end-effector of the robot. Also, B_d, C_d, K_d are the desired inertia, damping and stiffness matrices. The desired impedance of the robot is a design parameter [21]. The matrices $B_d,\ C_d,\ K_d$ are considered to be constant and diagonal; B_d must be positive definite and $C_d,\ K_d$ must be semi-positive definite [18]. From the robot dynamics in (6) we have

$$\ddot{q} = B^{-1}(\tau - \tau_{ext} - C\dot{q} - F_f - g) \tag{9}$$

Defining J as the Jacobian and using $\dot{x} = J\dot{q}$, the corresponding acceleration of the end-effector is

$$\ddot{x} = J\ddot{q} + \dot{J}\dot{q} \tag{10}$$

Putting (9) and (10) together results in:

$$\ddot{x} = JB^{-1}(\tau - \tau_{ext} - C\dot{q} - F_f - g) + \dot{J}\dot{q} \tag{11}$$

Using $\tau - \tau_{ext} = J^T(F - F_h)$, we have

$$\ddot{x} = JB^{-1}(J^T(F - F_h) - C\dot{q} - F_f - g) + \dot{J}\dot{q} \tag{12}$$

Defining $W = JB^{-1}J^T$, we have

$$\ddot{x} = W(F - F_h) - JB^{-1}(C\dot{q} + F_f + g) + \dot{J}\dot{q} \tag{13}$$

Then, F can be obtained as

$$F = W^{-1}\big(\ddot{x} + JB^{-1}(C\dot{q} + F_f + g) - \dot{J}\dot{q}\big) + F_h \tag{14}$$

Now, it is needed to consider (8) in the obtained equation. From (8) and defining $\tilde{x} = x_d - x$, we have

$$\ddot{x} = {B_d}^{-1}\big(- F_h + B_d\ddot{x}_d + C_d\dot{\tilde{x}} + K_d\tilde{x}\big) \tag{15}$$

putting (14) and (15) together, results in

$$F = W^{-1}\Big(B_d^{-1}(C_d\dot{\tilde{x}} + K_d\tilde{x}) + \ddot{x}_d + JB^{-1}(C\dot{q} + F_f + g) - \dot{J}\dot{q}\Big) + (I - W^{-1}{B_d}^{-1})F_h \quad (16)$$

therefore, $\tau = J^T F$ can be simplified as

$$\tau = J^T W^{-1}{B_d}^{-1}(C_d\dot{\tilde{x}} + K_d\tilde{x} + B_d\ddot{x}_d) + J^T(I - W^{-1}{B_d}^{-1})F_h + J^T W^{-1}JB^{-1}(C\dot{q} + F_f + g) - J^T W^{-1}\dot{J}\dot{q} \quad (17)$$

Finally, we have

$$\tau = B\ddot{q}^{+} + C\dot{q} + F_f + g + J^T F_h \quad (18)$$

where,

$$\ddot{q}^{+} = J^{-1}B_d^{-1}\big(B_d\ddot{x}_d + C_d\dot{\tilde{x}} + K_d\tilde{x} - B_d\dot{J}\dot{q} - F_h\big) \quad (19)$$

The obtained control law has been known as impedance control. If joint positions and velocities, and the external force values are available, (19) alongside (7) specifies the required actuator torques to impose the desired impedance to the robot end-effector.

3.3. Trajectory Generator

It has been proven that the human arm performs minimum jerk movements, where jerk is the changing rate of acceleration [22]. It means that the human arm movement minimizes the following objective function [23]

$$\Gamma = \int_0^{t_f} \Big(\frac{d^3x}{dt^3}\Big)^2 dt \quad (20)$$

where, t_f is the time duration of the movement. The considered function assures a smooth and safe movement for the human arm [22]. The trajectory that minimizes Γ is as [23]

$$x_d(t) = x_0 + (x_f - x_0)(6\xi^5 - 15\xi^4 + 10\xi^3) \quad (21)$$

where, $x_d = \begin{bmatrix}\boldsymbol{x}_d & z_d & \theta_d\end{bmatrix}^T$, $\xi = \frac{t}{t_f}$, x_0 and x_f are the end-effector position at initiating movement and when it stops moving at time t_f, respectively. Since the human operator cooperate with the robot when fine movements are required, the operator should be able to perform *lift*, *move*, and *slide* motion primitives as described thereafter.

3.3.1. Motion Primitives

The purpose of this section is to present the three considered motion primitives which are specified to simplify motion planning for glass panel installation [16]. The proposed motion primitives are defined as

- *Move*: To translate the glass panel horizontally until the top of the glass is almost underneath the top rail.

- *Slide*: To rotate the glass panel while maintaining both the horizontal position of the top of the glass, and the distance between the bottom of the glass panel and the floor until the glass is vertical.

- *Lift*: To lower the glass panel vertically when the glass is vertical.

The illustration of the three motion primitives is showed in the Fig. 4.

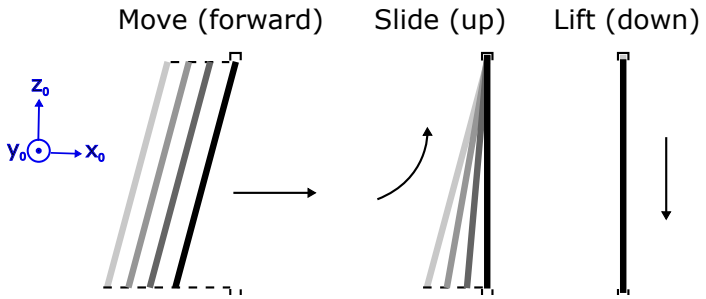

Figure 4: Illustration of the motion primitives *move*, *slide*, and *lift* [16].

As mentioned before, the defined motion primitives are used to make a trajectory that will serve as the input to the real-time position/velocity controllers. These motion primitives are defined as

$$\begin{aligned} &\bullet Move : x_{e,ref} = (\boldsymbol{x_0} + \varepsilon,\ z_0,\ \theta_0) \\ &\bullet Lift : x_{e,ref} = (\boldsymbol{x_0},\ z_0 + \varepsilon,\ \theta_0) \\ &\bullet Slide : x_{e,ref} = (\boldsymbol{x_0},\ z_0 + 2\delta_z(\cos(\theta_0 + \varepsilon) - \cos(\theta_0)),\ \theta_0 + \varepsilon) \end{aligned} \tag{22}$$

where, $x_e = (\boldsymbol{x}, z, \theta)$ denotes the configuration of the tool frame in the base frame. $\varepsilon \in \mathbb{R}$ is the path parameter, and $x_{e,ref}$ is the path from the initial configuration of the robot, i.e. $(\boldsymbol{x_0}, z_0, \theta_0)$. The defined motion primitives are used to make desired trajectories such that their difference with the

robot trajectory will serve as the input to the impedance controller. The robot trajectory can be obtained using the forward kinematic and Jacobian described thereafter.

3.4. Forward Kinematics and Jacobian

The forward kinematics of the robot is described in (3). The Jacobian, J, can be directly obtained from the kinematics as

$$J = \frac{\partial k(q)}{\partial q_i} = \begin{bmatrix} \frac{\partial \boldsymbol{x}}{\partial q_2} & \frac{\partial \boldsymbol{x}}{\partial q_3} & \frac{\partial \boldsymbol{x}}{\partial q_4} \\ \frac{\partial z}{\partial q_2} & \frac{\partial z}{\partial q_3} & \frac{\partial z}{\partial q_4} \\ \frac{\partial \theta}{\partial q_2} & \frac{\partial \theta}{\partial q_3} & \frac{\partial \theta}{\partial q_4} \end{bmatrix} \tag{23}$$

where,

$$\frac{\partial \boldsymbol{x}}{\partial q_2} = a_2 c_2$$

$$\frac{\partial \boldsymbol{x}}{\partial q_3} = -(d_6 + \delta_x) s_{34} + (\delta_z - a_5) c_{34} - a_4 s_3$$

$$\frac{\partial \boldsymbol{x}}{\partial q_4} = -(d_6 + \delta_x) s_{34} + (\delta_z - a_5) c_{34}$$

$$\frac{\partial z}{\partial q_2} = -a_2 s_2$$

$$\frac{\partial z}{\partial q_3} = -(d_6 + \delta_x) c_{34} - (\delta_z - a_5) s_{34} - a_4 c_3$$

$$\frac{\partial z}{\partial q_4} = -(d_6 + \delta_x) c_{34} - (\delta_z - a_5) s_{34}$$

$$\frac{\partial \theta}{\partial q_2} = 0$$

$$\frac{\partial \theta}{\partial q_3} = 1$$

$$\frac{\partial \theta}{\partial q_4} = 1$$

After calculating the forward kinematics and Jacobian, the position and velocity of the robot end-effector in the task space can be obtained as

$$\begin{aligned} x &= k(q) \\ \dot{x} &= J\dot{q} \end{aligned} \tag{24}$$

Then, their subtraction from the desired position and velocity of the robot are employed in the impedance controller.

3.5. Human Model

The human model block in the loop is used to detect the desired motion of the glass based on the operator's force. This motion will be interpreted as one of the three previously defined motion primitives. Human force exerted on the end-effector, F_h, can be written as

$$F_h = \begin{bmatrix} F_{hx} \\ F_{hz} \\ \tau_{hy} \end{bmatrix} \tag{25}$$

Then, the motion primitives can be chosen based on the following rules:

$$\text{Motion primitive} = \begin{cases} Move & , \|F_{hx}\| >> \|F_{hz}\| \\ Lift & , \|F_{hx}\| << \|F_{hz}\| \\ Slide & , \|F_{hx}\| < \|F_{hz}\| \end{cases} \tag{26}$$

The exact inequality relationship between $\|F_{hx}\|$ and $\|F_{hz}\|$, to choose between the motion primitives, can be found after experiments on the testbed of the robot, and a set of impedance parameters is associated with each motion primitive. After finding the desired motion primitive, the next step is to determine the human operator impedance. For modelling the human arm impedance, usually a linear second order system for small motions around the equilibrium point is consider as follows [24]:

$$B_h(\ddot{x} - \ddot{x}_v) + C_h(\dot{x} - \dot{x}_v) + K_h(x - x_v) = F_h \tag{27}$$

where, $B_h,\ C_h,\ K_h$ are the hand inertia, damping and stiffness matrices at virtual equilibrium position x_v, respectively [25]. Virtual equilibrium position x_v is the point where the net force acting on the mass is zero; x and F_h represent the end-effector position displacement and the human force applied to the end-effector of the robot with respect to to the human reference system [26], respectively. Considering $K_h = 0$ results in

$$B_h(\ddot{x} - \ddot{x}_v) + C_h(\dot{x} - \dot{x}_v) = F_h \tag{28}$$

Taking Laplace transformation results in

$$X(s) - X_v(s) = \frac{F_h(s)}{B_h s^2 + C_h s} = \frac{F_h}{C_h}\big(\frac{1}{s} - \frac{1}{s + \frac{C_h}{B_h}}\big) \tag{29}$$

which yields to

$$x(t) - x_v(T) = \frac{F_h}{C_h}\big(1 - \exp(-\frac{C_h}{B_h}t)\big) \tag{30}$$

The obtained $x(t) - x_v(t)$ can be used as $x_f - x_0$ in (21), at each time step. Then, t_f is

$$t_f = \frac{x_f}{v} \tag{31}$$

which v is the robot end-effector speed while collaborating with the human. To cope with safety requirements, the end-effector speed should not be completely dependent to the human arm speed but must be conform to an acceptable safe speed.

In the following, the simulation results for the proposed impedance controller are considered under different scenarios. In each scenario, it is assumed that the human operator aims to move the robot end-effector in the desired trajectories. The desired trajectories from the human operator are considered to be *lift*, *move*, and *slide* motions.

4. Simulation results

In this section, the results for the proposed online trajectory generation for impedance-controlled robots are provided. When there is no interaction between the human operator and the glass panel, the impedance is low in all three axes. When the human operator applies a force to the glass panel, the impedance parameters are changed to one of the predefined ones for each motion primitive. The robot continues moving based on these impedance parameters until the robot comes to a standstill. The simulations are done in Simulink/MATLAB 2017 and performed on a model of the WallMoBot, exported from Solidworks. The robot parameters used in the simulations are obtained from SolidWorks drawing and listed in Table 3. Since the considered robot is planar and rotates only around y_0, only the third elements of the moment of inertia of the elements between frame i and i+1, i.e., I_{zz_i} is needed. Moreover, since the elements between frames 3 and 4 only have translation motion and not rotational motion, I_{zz_3} is not needed. For the sake of safety,

the end-effector speed is assumed to be $v = 0.05\,\mathrm{m/s}$. The considered values for impedance coefficient are $B_h = 5,\ C_h = 23.5,\ K_h = 0$. To show the effectiveness of the proposed approach, the three motion primitives are tested.

Remark: When the robot end-effector moves according to one of the motion primitives, B_d and C_d are needed to be smaller to make the robot movement easier for that motion primitive. Also, K_d is needed to be larger to track the desired trajectory.

Table 3: Robot parameters, where COM_i and Izz_i are the relative position vector of the center of mass to the i^{th} joint, and the moment of inertia about the z-axis of the elements between frame i and $i+1$ relative to the coordinate frame i, respectively, and m_i is the mass of these elements.

i	COM_i [m]	m_i [kg]	Izz_i [kg.m^2]
2	$[0.260; 0; 0.041]^T$	3.31	0.309
3	$[0.683; -0.008; 0.041]^T$	10.42	–
4	$[0.440; -0.008; 0.028]^T$	6.21	1.624
5	$[0.089; -0.317; 0.027]^T$	177	69.79

4.1. Lift

In this section, we assume that $\|F_{hx}\| << \|F_{hz}\|$. It means the human operator performs the lift motion, i.e., a movement in the z-direction. Based on (21), the minimum jerk trajectory in z-direction is

$$z_d(t) = z_0 + (z_f - z_0)(6\xi^5 - 15\xi^4 + 10\xi^3) \tag{32}$$

where, z_0 and z_f are the glass position at z-direction at time t_0 and t_f respectively. The impedance parameters in (8) are set as follows :

$$\begin{aligned} B_d = \begin{bmatrix} 15 & 0 & 0 \\ 0 & 0.1 & 0 \\ 0 & 0 & 1 \end{bmatrix},\ C_d = \begin{bmatrix} 200 & 0 & 0 \\ 0 & 100 & 0 \\ 0 & 0 & 100 \end{bmatrix}, \\ K_d = \begin{bmatrix} 400 & 0 & 0 \\ 0 & 6000 & 0 \\ 0 & 0 & 100 \end{bmatrix} \end{aligned} \tag{33}$$

The simulation is done considering the human operator moves the glass panel 10 cm in the z-direction. The simulation result is shown in Fig. 5

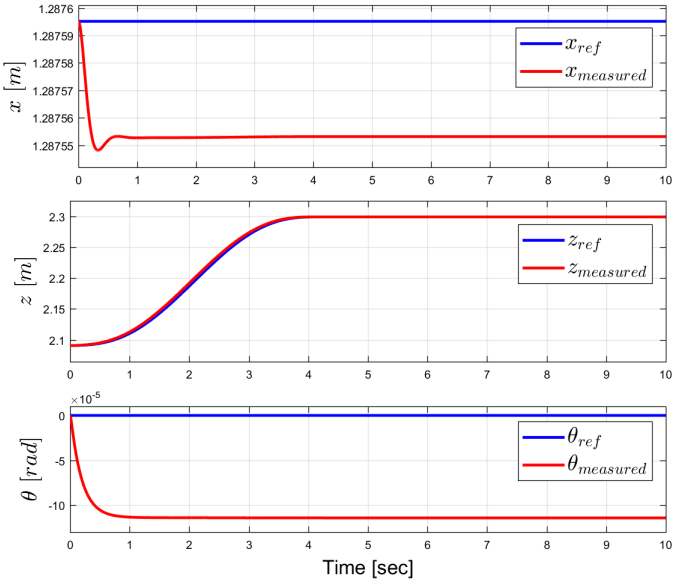

Figure 5: Illustration of the end-effector position using the impedance controller when the human operator moves the glass panel in the z-direction.

which shows that the robot end-effector reaches the desired position with the desired transient dynamics, and thus the impedance controller performs well in the lift motion.

4.2. Move

Now, we assume that $\|F_{hx}\| >> \|F_{hz}\|$. It means that the human operator performs the move motion, i.e., a movement in the x-direction. Based on (21), the minimum jerk trajectory in $\boldsymbol{x}$-direction is as

$$\boldsymbol{x}_d(t) = \boldsymbol{x}_0 + (\boldsymbol{x}_f - \boldsymbol{x}_0)(6\xi^5 - 15\xi^4 + 10\xi^3) \tag{34}$$

where, $\boldsymbol{x}_0$ and $\boldsymbol{x}_f$ are the glass position in $\boldsymbol{x}$-direction at time t_0 and t_f respectively. The impedance parameters in (8) are set as follows:

$$B_d = \begin{bmatrix} 0.1 & 0 & 0 \\ 0 & 15 & 0 \\ 0 & 0 & 1 \end{bmatrix}, \quad C_d = \begin{bmatrix} 100 & 0 & 0 \\ 0 & 200 & 0 \\ 0 & 0 & 100 \end{bmatrix}, \quad K_d = \begin{bmatrix} 6000 & 0 & 0 \\ 0 & 400 & 0 \\ 0 & 0 & 100 \end{bmatrix} \tag{35}$$

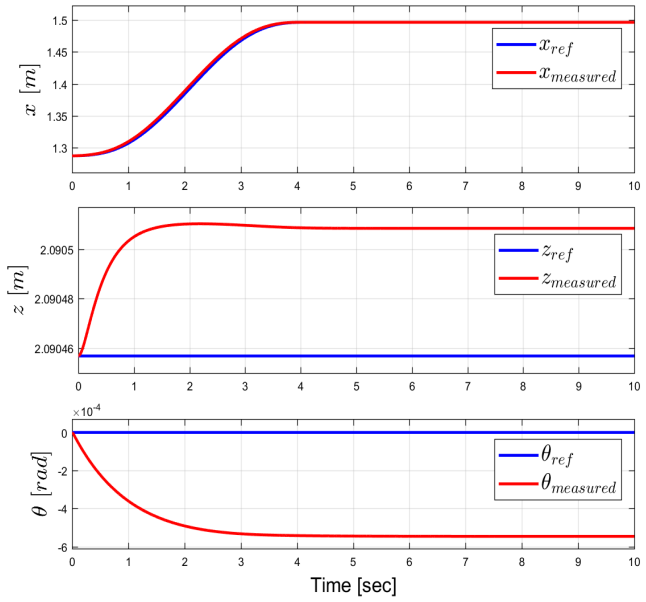

Figure 6: Illustration of the end-effector position using the impedance controller when the human operator moves the glass panel in the $\boldsymbol{x}$-direction.

The performance of the proposed approach when the human operator moves the glass panel 10 cm in the $\boldsymbol{x}$-direction is depicted in Fig. 6. It can be seen that the robot end-effector follows the desired trajectory in $\boldsymbol{x}$-direction while the robot end-effector movement in other directions is almost zero, which is the expected performance of the impedance controller.

4.3. Slide

Finally, we assume that $\|F_{hx}\| < \|F_{hz}\|$, which means the human operator performs the slide motion. Based on (21) and (22), the minimum jerk trajectory is as

$$\begin{aligned} \theta_d(t) &= \theta_0 + (\theta_f - \theta_0)(6\xi^5 - 15\xi^4 + 10\xi^3) \\ z_d(t) &= z_0 + \delta_h(6\xi^5 - 15\xi^4 + 10\xi^3) \end{aligned} \tag{36}$$

where,

$$\delta_h = 2\delta_z\big(\cos(\theta_f) - \cos(\theta_0)\big)$$

where, θ_0 and θ_f are the angle between the top of the glass panel and the vertical line at time t_0 and t_f, respectively, while having the same distance between the bottom of the glass panel and the ground, and δ_z is the height of the glass panel from the attachment point to the top. The impedance parameters in (8) are set as follows:

$$\begin{aligned} B_d = \begin{bmatrix} 10 & 0 & 0 \\ 0 & 0.5 & 0 \\ 0 & 0 & 0.5 \end{bmatrix}, \quad C_d = \begin{bmatrix} 100 & 0 & 0 \\ 0 & 50 & 0 \\ 0 & 0 & 5 \end{bmatrix}, \\ K_d = \begin{bmatrix} 100 & 0 & 0 \\ 0 & 4000 & 0 \\ 0 & 0 & 400 \end{bmatrix} \end{aligned} \tag{37}$$

In this scenario, it is considered that the human operator performs the *slide* movement. As can be seen from (37), the main changes in this movement happen in θ direction while z changes slightly and $\boldsymbol{x}$ remains constant. The simulation result is shown in Fig. 7, which shows that with the proposed impedance controller the robot end-effector reaches the desired position with the desired transient dynamics.

5. Conclusion

In the research reported in this paper, a novel impedance controller that is interconnected to an online trajectory generator is employed on the Wall-MoBot. The trajectory generation algorithm copes with safety concerns, and the impedance controller is designed such that the tracked trajectory of the

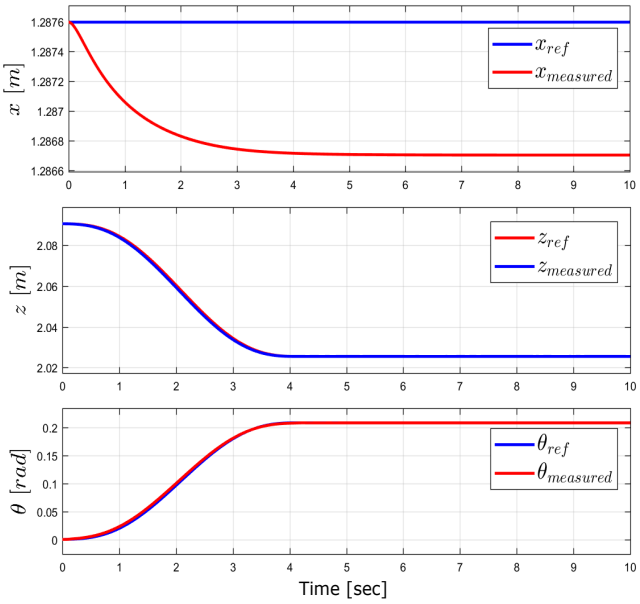

Figure 7: Illustration of the end-effector position using the impedance controller when the human operator moves the glass panel as the slide movement.

robot end-effector, which is caused by the human operator intention, automatically selects between the defined motion primitives for WallMoBot, i.e. *move*, *slide*, *lift*. The simulation results showed the ability of the proposed impedance controller in tracking the desired trajectories of the human operator. For future work, we plan to implement the proposed approach in an experimental framework.

6. Acknowledgements

This research was supported by Innovation Fund Denmark in project number 5150-00007A called WallMoBot. We are thankful to our colleagues in the University of Southern Denmark (SDU) who provided the computer-aided design (CAD) models for the WallMoBot in Figs. 1 and 2. We are also grateful to WallMo A/S for assistance with the project.

References

[1] Hersh, M.: 'Overcoming barriers and increasing independence–service robots for elderly and disabled people', *International Journal of Ad-*

vanced Robotic Systems, 2015, **12**, (8), pp. 114

[2] Butner, S.E., Ghodoussi, M.: 'Transforming a surgical robot for human telesurgery', *IEEE Transactions on Robotics and Automation*, 2003, **19**, (5), pp. 818–824

[3] Wen, R., Tay, W.L., Nguyen, B.P., Chng, C.B., Chui, C.K.: 'Hand gesture guided robot-assisted surgery based on a direct augmented reality interface', *Computer methods and programs in biomedicine*, 2014, **116**, (2), pp. 68–80

[4] Siciliano, B., Khatib, O., editors. 'Springer Handbook of Robotics'. (Springer Berlin Heidelberg, 2008)

[5] Luttmann, A., Jager, M., Griefahn, B., Caffier, G., Liebers, F., Organization, W.H., et al.: 'Preventing musculoskeletal disorders in the workplace', 2003

[6] Wang, X.V., Kemény, Z., Váncza, J., Wang, L.: 'Human–robot collaborative assembly in cyber-physical production: Classification framework and implementation', *CIRP Annals-Manufacturing Technology*, 2017

[7] Calanca, A., Muradore, R., Fiorini, P.: 'A review of algorithms for compliant control of stiff and fixed-compliance robots', *IEEE/ASME Transactions on Mechatronics*, 2016, **21**, (2), pp. 613–624

[8] Surdilovic, D. 'Contact stability issues in position based impedance control: Theory and experiments'. In: IEEE International Conference on Robotics and Automation, 1996, vol. 2, pp. 1675–1680

[9] Part, S.: 'Impedance control: An approach to manipulation', *Journal of dynamic systems, measurement, and control*, 1985, **107**, pp. 17

[10] Gu, J. 'Development of impedance sensing technology and an intelligent control system for robot-automated processing of flexible and natural objects'. University of British Columbia, 1999

[11] Méndez, J.d.D.F., Schiøler, H., Madsen, O., Bai, S. 'Impedance control of a redundant parallel manipulator'. In: The 14th International Conference on Informatics in Control, Automation and Robotics. (SCITEPRESS Digital Library, 2017. pp. 104–111

[12] Sosnik, R., Hauptmann, B., Karni, A., Flash, T.: 'When practice leads to co-articulation: the evolution of geometrically defined movement primitives', *Experimental Brain Research*, 2004, **156**, (4), pp. 422–438

[13] Kulvicius, T., Ning, K., Tamosiunaite, M., Worgötter, F.: 'Joining movement sequences: Modified dynamic movement primitives for robotics applications exemplified on handwriting', *IEEE Transactions on Robotics*, 2012, **28**, (1), pp. 145–157

[14] Schöllig, A., Hehn, M., Lupashin, S., D'Andrea, R. 'Feasiblity of motion primitives for choreographed quadrocopter flight'. In: American Control Conference (ACC), 2011. (IEEE, 2011. pp. 3843–3849

[15] Murali, A., Sen, S., Kehoe, B., Garg, A., McFarland, S., Patil, S., et al. 'Learning by observation for surgical subtasks: Multilateral cutting of 3d viscoelastic and 2d orthotropic tissue phantoms'. In: IEEE International Conference on Robotics and Automation (ICRA), 2015. pp. 1202–1209

[16] Sloth, C., Pedersen, R. 'Control of wall mounting robot'. In: Proceedings of the 20th World Congress of the International Federation of Automatic Control (IFAC), 2017

[17] Cousineau, L., Miura, N.: 'Construction robots: the search for new building technology in Japan'. (ASCE Publications, 1998)

[18] Jlassi, S., Tliba, S., Chitour, Y. 'An online trajectory generator-based impedance control for co-manipulation tasks'. In: IEEE Haptics Symposium (HAPTICS), 2014, pp. 391–396

[19] Slotine, J.J.E., Li, W., et al.: 'Applied nonlinear control'. vol. 199. (Prentice hall Englewood Cliffs, NJ, 1991)

[20] Lewis, F.L., Dawson, D.M., Abdallah, C.T.: 'Robot manipulator control: theory and practice'. (CRC Press, 2003)

[21] Lu, W.S., Meng, Q.H.: 'Impedance control with adaptation for robotic manipulations', *IEEE Transactions on Robotics and Automation*, 1991, **7**, (3), pp. 408–415

[22] Flash, T., Hogan, N.: 'The coordination of arm movements: an experimentally confirmed mathematical model', *Journal of neuroscience*, 1985, **5**, (7), pp. 1688–1703

[23] Rahman, M., Ikeura, R., Mizutani, K. 'Investigating the impedance characteristic of human arm for development of robots to co-operate with human operators'. In: IEEE International Conference on Systems, Man, and Cybernetics, vol. 2, pp. 676–681

[24] Dolan, J.M., Friedman, M.B., Nagurka, M.L.: 'Dynamic and loaded impedance components in the maintenance of human arm posture', *IEEE Transactions on Systems, Man, and Cybernetics*, 1993, **23**, (3), pp. 698–709

[25] Gu, X., Ballard, D.H. 'An equilibrium point based model unifying movement control in humanoids.'. In: Robotics: science and systems, 2006.

[26] Artemiadis, P.K., Katsiaris, P.T., Liarokapis, M.V., Kyriakopoulos, K.J. 'Human arm impedance: Characterization and modeling in 3d space'. In: IEEE/RSJ International Conference on Intelligent Robots and Systems (IROS), 2010, pp. 3103–3108